HOKKAIDO UNIVERSITY

Title	Assessment of canopy photosynthetic capacity and estimation of GPP by using spectral vegetation indices and the light–response function in a larch forest
Author(s)	Ide, Reiko; Nakaji, Tatsuro; Oguma, Hiroyuki
Citation	Agricultural and Forest Meteorology, 150(3), 389-398 https://doi.org/10.1016/j.agrformet.2009.12.009
Issue Date	2010-03-15
Doc URL	http://hdl.handle.net/2115/47002
Type	article (author version)
File Information	AFM150-3_389-398.pdf

Instructions for use

Hokkaido University Collection of Scholarly and Academic Papers : HUSCAP

Assessment of canopy photosynthetic capacity and estimation of GPP by using spectral vegetation indices and the light–response function in a larch forest

Reiko Ide[a,*], Tatsuro Nakaji[b], and Hiroyuki Oguma[a]

[a]National Institute for Environmental Studies,16-2 Onogawa, Tsukuba, 305-8506, Japan

[b]Field Science Center for Northern Biosphere, Hokkaido University, Tomakomai, Hokkaido, Japan

*Corresponding author: Tel.: +81 29 850 2976; fax: +81 29 850 2960.

E-mail address: ide.reiko@nies.go.jp

ABSTRACT

Integration of CO_2 flux observations with remote sensing technique and ecosystem modeling is expected to be useful for estimation of gross primary production (GPP). We focused on the changes in the two main parameters for the canopy-scale light–response curve—P_{max} (maximum GPP at light saturation) and ϕ (initial slope)—as indicators to represent canopy photosynthetic capacity. We hypothesized that P_{max} and ϕ could be evaluated by using spectral reflectance related to the changes in the levels of canopy nitrogen and chlorophyll. We analyzed the relationships between P_{max} and ϕ, derived from tower-based CO_2 flux observations, and ground-based spectral vegetation indices (VIs) in a temperate deciduous coniferous forest.

The canopy-scale P_{max} and ϕ showed clear seasonal changes accompanying phenological stages. Both the variations in P_{max} and ϕ were strongly correlated with VIs, especially with the ratio vegetation index (RVI) and enhanced vegetation index (EVI), independent of the growth stages. Moreover, day-to-day short-term variations of P_{max} and ϕ were affected by meteorological conditions such as vapor pressure

deficit (VPD) and relative solar radiation which was calculated as the ratio of monitored radiation per theoretical maximum radiation.

Thus, seasonal changes of P_{max} and ϕ were effectively assessed by RVI or EVI, and their short-term variations were evaluated by the empirical relationships with VPD and relative solar radiation. We propose a new simple method for estimating GPP with good precision; by fitting the light–response function with the evaluated parameters, the estimated GPP reflects 3 types of temporal variation: diurnal, day-to-day, and seasonal.

Keywords: GPP, light–response curve, maximum photosynthesis (P_{max}), initial slope (ϕ), spectral vegetation index, vapor pressure deficit (VPD), relative solar radiation, eddy covariance

1. Introduction

Estimating the uptake of CO_2 by terrestrial ecosystems is an important consideration in the forecasting of global warming. The eddy covariance method is used worldwide to measure CO_2 flux as a precise means for continuous measurement of CO_2 exchange. The data have accumulated in recent years, and regional comparison studies are being performed (e.g., Falge et al., 2002; Saigusa et al., 2008). To estimate CO_2 exchange over wide areas, the CO_2 flux measurements from distributed points must be scaled up to spatially continuous estimates. Remote sensing technique and terrestrial ecosystem models should be useful for this purpose. Because satellite remote sensing allows simultaneous repetitive observations over wide areas, information can be obtained with extensive temporal and spatial coverage. The spectral data from optical remote sensing can be used to evaluate parameters in ecological models based on photosynthetic mechanisms. The spectral data should reflect physiological characteristics independent of vegetation types or growth stages.

One of the methods that utilize remote sensing data to estimate GPP is the light use efficiency (LUE) model (Monteith, 1972, 1977; Prince and Goward, 1995). The LUE model expresses GPP as the product of absorbed photosynthetically active radiation (APAR) and the LUE. APAR is calculated by multiplication of observed incident PAR by the fraction of absorbed PAR (FAPAR), which is estimated from vegetation indices (VIs) such as the normalized difference vegetation index (NDVI) or the enhanced vegetation index (EVI), obtained by remote sensing (e.g., Huete et al., 2002). However, the relationship between FAPAR and NDVI shows seasonal hysteresis, being affected by phenological stages (Jenkins et al., 2007). On the other hand, although the LUE, the ratio of GPP to APAR, is often estimated by using VIs such as photochemical reflectance index (PRI) (Nichol et al., 2006; Nakaji et al., 2008), there are some problems on the estimation of LUE from VIs in the whole time scales. The LUE is affected by light environments such as variations in radiation intensity and sky condition (Sims et al. 2005; Nakaji et al. 2007).

The phenological development of vegetation strongly affects GPP of deciduous forests (Saigusa et al., 2008). Temporal variations of photosynthetic capacity and efficiency at canopy scale have not been adequately assessed in many models, even though the evident seasonal changes of those at leaf scale are shown (Muraoka and Koizumi, 2005). Therefore, our objective in this study was to assess the variations of canopy photosynthetic capacity and efficiency using spectral information and a plant physiological approach, to allow a scale-up of tower-based CO_2 flux observation data to a CO_2 balance over wide areas. For this purpose, we focused on the light–response function at canopy scale and variations of its two main parameters, the maximum GPP under light saturation (P_{max}) and the initial slope (ϕ) of light–response curve, instead of on LUE and FAPAR.

A number of physiological studies at foliage scale have pointed out that the maximum photosynthetic capacity (A_{max}) is correlated with leaf nitrogen (N) level (Reich et al., 1995, 1999). Furthermore, the correlations between mass-based A_{max} and mass-based N can be described with one general equation independent of plant functional type or biome (Wright et al., 2004). Also, the initial slope of the light–response curve is related to chlorophyll concentration, which is associated with the electron transport rate. Remote sensing studies have proven that foliage N and chlorophyll content are evident in the spectral reflectance (e.g., Yoder and Pettigrew-Crosby, 1995). Therefore, we hypothesized that P_{max} and ϕ could be evaluated by using spectral reflectance as related to changes in canopy N and chlorophyll levels.

However, due to the limit of temporal and spatial resolution of remote sensing, it is difficult to detect short-term responses of plants or small physiological changes, such as stomatal conductance. Then we analyzed the relationship between day-to-day short-term variations of P_{max} and ϕ with daily meteorological conditions. We combined our results for both seasonal and short-term variations to estimate the canopy-scale P_{max} and ϕ, and thereby demonstrate and validate a new method for estimating GPP by using spectral vegetation indices and the light–response function.

2. Background and hypothesis

2.1. Light–response curve, P_{max} and ϕ

P_{max} and ϕ at canopy scale, as at leaf scale, are important parameters of photosynthesis, and they can be calculated from CO_2 flux measurements (Ruimy et al., 1995). GPP is obtained as the sum of net ecosystem production (NEP) and ecosystem respiration (RE):

$$\mathrm{GPP} = \mathrm{NEP} + \mathrm{RE} \quad (1)$$

Here, NEP is assumed equal to the negative of net ecosystem CO_2 exchange (NEE). GPP has been approximated as a function of PAR by the light–response curve. Curve-fitting of the light–response curve by using rectangular hyperbolic functions is generally used as an effective method to gap-fill for missing values in NEE (Falge et al., 2001). Also the non-rectangular hyperbolic equation (Thornley, 1976) is widely applied for gap-filling of NEE (Kosugi et al., 2005; Saigusa et al., 2008), and for predicting canopy photosynthesis (e.g., Saito et al., 2009). We compared these equations and selected the following non-rectangular hyperbolic equation to estimate GPP because of the best fit to GPP among them at this site (Appendix A):

$$\mathrm{GPP} = \frac{\phi \cdot \mathrm{PAR} + P_{max} - \sqrt{\left(\phi \cdot \mathrm{PAR} + P_{max}\right)^2 - 4\phi \cdot \mathrm{PAR} \cdot \theta \cdot P_{max}}}{2\theta} + Rd \quad (2)$$

Here, P_{max} (μmol CO_2 m^{-2} s^{-1}) is the maximum GPP at light saturation, ϕ (mol CO_2 [mol photon]$^{-1}$) is the initial slope of the curve, and θ represents the convexity of the curve. Rd (μmol CO_2 m^{-2} s^{-1}) is daytime respiration.

2.2 Vegetation indices

We analyzed the relationships between photosynthetic parameters and several indices (Table 1). NDVI, EVI, and the ratio vegetation index (RVI) are indices for green leaf quantity based on

Table 1

differences in reflectance between red and near-infrared bands. Chlorophyll has high absorbance in the visible red wavelength region (around 630–690 nm), whereas there is strong reflectance from cell walls and intracellular water of plants in the near-infrared region (around 740–900 nm). Thus, an increase in the quantity of healthy green leaves is accompanied by a decrease in red reflectance and a rise in near-infrared reflectance. RVI is a simple ratio of the reflectance of red and near-infrared bands.

NDVI is widely used for assessing parameters such as the vegetation cover ratio, leaf area index (LAI), and FAPAR (e.g., Sellers et al., 1992; Potter et al., 1993; Myneni et al., 1997); however, because it is a normalized index, it has the disadvantage of saturating at high biomass (Goward and Huemmrich, 1992). EVI corrects this disadvantage and can indicate the status of vegetation with mitigating effects of aerosols and soil by incorporating the reflectance for blue wavelengths (Huete et al., 2002). We anticipated that EVI and RVI could detect the canopy photosynthetic capacity as indices for N content.

The photochemical reflectance index (PRI) has been proposed as an optical indicator for detecting epoxidation and de-epoxidation changes of xanthophyll related to heat dissipation (Gamon et al., 1997). This index is calculated from the reflectance on both sides of the green absorbance band (531 and 570 nm). It also corresponds to the carotenoid:chlorophyll pigment ratio (Sims and Gamon, 2002). In this study, we expected that PRI might detect the "daytime depression" phenomenon during foliage period as well as autumn color changes (Nakaji et al., 2006).

The canopy chlorophyll index (CCI) has been proposed as an index for reflecting changes in chlorophyll content through the red edge shift (Sims et al., 2006). CCI is calculated by the ratio of the first derivatives of reflectance at wavelengths around the red edge (700 and 720 nm).

2.3 Summary of GPP estimation methods

Various environmental (stress) factors affect the photosynthetic rate of larch canopy. Diurnal and daily changes in GPP are mainly controlled by irradiance, as expressed by the light–response curve. The photosynthetic capacity P_{max} and ϕ, which regulate the light–response curve, have seasonal trends in relation to the seasonality in temperature and LAI. Spectral vegetation indices are expected to

reflect these seasonal trends in relation to the changes in canopy N level. Moreover, photosynthetic capacity would be affected by daily environmental conditions such as temperature, VPD, and soil water.

Therefore, our goal was to provide a precise estimation of GPP with a combination of 3 types of temporal resolution: (1) seasonal variation, by using VIs; (2) short-term variation, by using meteorological factors; and (3) diurnal variation, by using the light–response function (Fig. 1).

Fig. 1

First, we assessed the seasonality of the parameters using VIs in Process 1. From the relationships with the VIs (VI_1 and VI_2, showing the best correlations with P_{max} and ϕ, respectively), seasonal variations for daily-scale P_{max} (P_{max_season}) and ϕ ($\phi_{\_season}$) could be empirically described as:

$$P_{max\_season} = f_1(VI_1), \qquad \phi_{\_season} = f_2(VI_2) \tag{3}$$

In addition to the seasonality of the parameters, we defined ΔP_{max} and $\Delta\phi$ as the day-to-day short-term variations in daily P_{max} and ϕ. These were expressed as differences between the approximated original parameters (P_{max} and ϕ in Eq. 2) and the estimated seasonal parameters (P_{max_season} and $\phi_{\_season}$ in Eq. 3) as follows:

$$\Delta P_{max} = P_{max} - P_{max\_season},$$

$$\Delta\phi = \phi - \phi_{\_season} \tag{4}$$

ΔP_{max} and $\Delta\phi$ were expressed as empirical functions of meteorological factors in Process 2. Then, the estimated daily P_{max} and ϕ (est_P_{max}, est_ϕ) were determined as the sums of seasonal and short-term variations of parameters.

Finally in Process 3, GPP was estimated by fitting the daily fluctuating parameters est_P_{max} and est_ϕ, Rd and PAR to the light–response function (Eq. 2). When half-hourly PAR data are used, half-hourly GPP estimates are obtained.

3. Methods

3.1 Study site

The study site was a temperate deciduous coniferous forest at Tomakomai Flux Research Site (lat. 42°44′N, long. 141°31′E, 125 m above sea level), in the northern part of Japan. About 81% of the approximately 100-ha site was dominated by a stand of Japanese larch (*Larix kaempferi*). The trees were about 45 years old, 15 m tall, with mean diameter at breast height (DBH) of 19 cm. Other trees on the site included deciduous trees such as birch (*Betula ermanii*, *B. platyphylla*) and Japanese elm (*Ulmus japonica*) mixed with evergreen conifer species such as spruce (*Picea jezoensis*). The forest floor was thickly covered with Japanese spurge (*Pachysandra terminalis*), ferns (*Dryopteris crassirhizoma*), and other species.

The maximum LAI for the canopy was 5.6 m^2 m^{-2} and for the lower-layer vegetation, 3.6 m^2 m^{-2}, for a total maximum of 9.2 m^2 m^{-2}, as determined by a leaf collection method. The seasonal change of LAI was estimated from Beer's law using an extinction coefficient of 0.58 and a plant area index of 1.4 m^2 m^{-2} (Hirata et al., 2007). The soil was a highly permeable oligotrophic Regosol of volcanic origin (Fujinuma et al., 2001). The mean air temperature was 6.2 °C and mean annual precipitation was 1043 mm during 2001–2003.

The flux tower and forest at the site were completely destroyed by a typhoon on 8 September 2004.

3.2 Measurement of CO_2 flux and micrometeorological parameters

CO_2 flux (F_c) was measured using the eddy covariance technique with a closed-path infrared gas analyzer (Li6262; Li-Cor, Lincoln, Nebraska, USA); wind velocity and air temperature were measured simultaneously using a three-dimensional sonic anemometer-thermometer (DA-600-3TV; Kaijo, Tokyo, Japan) at 27 m on the tower. The sampled air was drawn from an inlet at 27-m height and pumped into the gas analyzer. Raw data were recorded at 10 Hz using a data logger (DR-M3; TEAC, Tokyo, Japan). CO_2 measurements were calibrated once a day by flowing two CO_2 standard

gases of 320 and 420 ppmv (Hirano et al., 2003). After removal of noise spikes, corrections were applied for three-dimensional coordinate rotation, for time lag, and for air density fluctuations, and then half-hourly mean values for F_c were calculated. In addition, the rate of change in CO_2 storage (F_s) below the F_c measurement height was obtained from the vertical profile of CO_2 concentrations at eight levels.

Net ecosystem exchange (NEE) was calculated as the sum of F_c and F_s:

$$NEE = F_c + F_s \tag{5}$$

Meteorological factors such as global solar radiation, PAR, air temperature, precipitation on the flux tower, soil temperature, and soil water content were measured. As we did not monitor diffuse solar radiation, for this study we substituted the relative solar radiation (rSR). We defined rSR as the ratio of observed irradiance to theoretical irradiance of full sunlight, which was estimated from the solar zenith angle at the time, atmospheric turbidity, albedo, and precipitable water vapor (Kondo and Miura, 1983). We distinguished clear sky and cloudy conditions in this study by values of rSR ≥ 75% or rSR < 75%, respectively.

3.3 Calculation of photosynthetic parameters

The data from January 2003 to August 2004 were available for analysis. When the friction velocity (u*) was less than 0.3 m s^{-1}, nighttime F_c tended to be underestimated at this site (Hirata et al., 2007), so under these conditions the values for NEE were excluded. NEE during nighttime and winter snowfall periods was assumed to be equal to RE. The observed RE was regressed using the equation of Lloyd and Taylor (1994):

$$RE = RE_{ref} \exp\left\{\frac{E_0}{R}\left(\frac{1}{T_k + T_{ref} - T_0} - \frac{1}{T_k + T_s - T_0}\right)\right\} \tag{6}$$

Here, RE_{ref} is the ecosystem respiration rate (μmol CO_2 m^{-2} s^{-1}) at the reference temperature (10 °C), E_0 is activation energy (J mol^{-1}), R is the gas constant (R = 8.314 J mol^{-1} K^{-1}), T_s is the soil temperature (°C, 0.05 m depth), and T_0 and T_k are constants with T_0 = 273.15 K and T_k = 227.13 K. The two regression parameters, RE_{ref} and E_0, were determined each day with a 91-day moving window, considered to reflect the seasonality of RE. Gaps in nighttime RE were filled and daytime RE was estimated from the soil temperature by fitting Eq. 6. GPP was then calculated by using Eq. 1.

GPP was fitted to the light–response curve (Eq. 2) with a 3-day (2 previous days included) moving window throughout a year, and the daily parameters P_{max} (μmol CO_2 m^{-2} s^{-1}), ϕ (mol CO_2 [mol photon]$^{-1}$), and Rd (μmol CO_2 m^{-2} s^{-1}) were determined. Here, the convexity (θ) of the light–response curve was set at 0.9, following previous studies (Kosugi et al., 2005; Saigusa et al., 2008; Saito et al., 2009). The Gauss-Newton least-squares method was used in the non-linear regression. Although a regression period of approximately 10 days is recommended for use in flux gap-filling (Falge et al., 2001; Baldocchi and Wilson, 2001), we used a moving window of 3 days to investigate the short-term effects of weather conditions. Because weather conditions showed a 3- or 4-day cycle variation especially in spring in Japan due to migratory High (e.g., Nemoto et al., 1982). The window size of 3 days was sufficiently short to remove seasonal effects and was long enough to provide sufficient data points for stable regression analysis.

Parameter values were excluded from analysis when the number of valid data points were too few for regression analysis (<20 for a 3-d period), when convergence was impossible (the coefficient of determination [r^2] was less than 0.1), when the parameters were out of range ($P_{max} \geq 50.0$ or ≤ 0.1 μmol CO_2 m^{-2} s^{-1}; $\phi \geq 1.0$ or ≤ 0.001 mol CO_2 [mol photon]$^{-1}$), or when PAR was too low to reach light saturation.

3.4 Spectral reflectance and vegetation indices

Upward and downward spectral radiation was observed with two grating spectroradiometers (MS-700; EKO Instruments, Tokyo, Japan) mounted on the tower at 40-m height. Spectral radiation for 256 wavelength bands ranging from 305 to 1150 nm at about 3.3-nm intervals was measured every

minute, and the spectral reflectance of larch canopy was derived from the upward radiation divided by the downward radiation. Both spectroradiometers were simultaneously calibrated once a year for the radiation level of each band.

Each VI was calculated from the averaged spectral reflectance at three bands around each wavelength in Table 1. We used the data for half-hourly mean values around noon as the representative values for each day. If there was rain within the preceding 12 hours, the data were excluded from the analysis. Assuming the proposed application of this method for satellite remote sensing, we only used the data from under clear sky conditions (rSR > 75%, see Section 3.2).

3.5 Data set

In this study, we used the data of CO_2 flux, meteorological parameters and spectral reflectance which were collected from January 2003 to August 2004, just before the destruction of the tower. In order to analyze the seasonal variation of the photosynthetic parameters and VIs, the data from the autumn of 2003 were added as a continuation after August 2004. We selected 50% of the days at random for "training data" to construct the model, and used the rest of the data set as "test data" to examine the model validity.

3.6 Monitoring of phenology

To compare the seasonal changes in P_{max} and ϕ with the actual phenology of the vegetation, we visually assessed the phenology by using photographic images from digital cameras mounted on the flux tower.

The Japanese larch has two types of shoots: short-shoots and long-shoots. First, buds of the short-shoots break and grow, developing their leaves on the old branches of the previous year, which here we call leaf "flush". Subsequently, the long-shoots grow from the tips of the previous year’s branches.

4. Results and discussion

4.1 Seasonal variations in P_{max} and ϕ

Clear seasonal variations of canopy P_{max} and ϕ were observed related to changes in the vegetation phenology (Fig. 2). The flush of leaves in the larch forest started at the end of April, about 2 weeks after the disappearance of snow, and short-shoot leaves had developed for about 3 weeks. Both P_{max} and ϕ increased along with the flush of leaves.

Fig. 2

From mid-June to the beginning of August, long-shoots elongated. P_{max} and ϕ continued to increase and reached their maximum values at the end of June, during the elongation period. P_{max} and ϕ gradually decreased from August with large daily fluctuations, while temperature and LAI remained at their maximum levels.

The leaf color change started in mid-October and reached peak coloration at the end of October. The leaves had fallen within the first 10 days of November. P_{max} and ϕ continued to decline, reaching minimum values during the period of leaf color change.

4.2 Seasonal variations of vegetation indices (VIs)

Each VI had a different seasonal pattern, with different times of increase, maximum, and decrease (Fig. 3). At the time of snow disappearance, NDVI showed a jump up from its minimum level, and EVI and RVI rose a little, on the contrary PRI dropped down. NDVI sensitively reflected the condition of the ground surface. NDVI, EVI, and RVI increased linearly over 1 month just after the start of flush, whereas PRI and CCI increased more gradually over 2 months. Although NDVI maintained maximum values over 2 months during summer, EVI and RVI had shorter periods of maximum values, from mid-June to July. In early July of 2004, after a few days of heavy rain and low temperatures, LAI decreased even though it was still the leaf extension period (Fig. 2). VIs except for NDVI detected this

Fig. 3

change and decreased at the same time (Fig. 3). NDVI became saturated during summer and did not follow the decrease of LAI.

PRI and CCI peaked in late summer in 2003. Whereas EVI and RVI declined gradually from late summer, PRI declined later, in early autumn. PRI would be affected by the decrease of chlorophyll and the increase of carotenoid pigments (Sims and Gamon, 2002) and is therefore more sensitive to senescence than other VIs. PRI had greater daily fluctuation than the other VIs. In early June, ϕ decreased during a few sunny days, and the drop was followed only by PRI. The strong solar radiation probably caused de-epoxidation of xanthophyll pigments for photoprotection, which was possibly detected by PRI (Gamon et al., 1992; Nakaji et al., 2006). PRI showed the unique pattern of declining in autumn far below the spring baseline and rising again during winter.

4.3 Relationships of P_{max} and ϕ to VIs

P_{max} and ϕ were significantly correlated with VIs, LAI and temperature, and the correlations with VIs were higher than with LAI or temperature (Table 2). P_{max} was strongly correlated with EVI and RVI (r = 0.92 for both). NDVI and P_{max} had an exponential relationship, because NDVI saturated during the period of maximum P_{max}. PRI showed a lower correlation with P_{max} because of its different pattern of decline in autumn.

Table 2

ϕ had highest correlation with RVI (r = 0.81) and next highest with EVI (r = 0.79), and the correlation between P_{max} and ϕ was relatively high (r = 0.74, data not shown). NDVI, PRI, and CCI had lower correlations with ϕ, owing to different peak periods and patterns of decline. Variations of both ϕ and PRI coincided well only during the period from spring to summer.

Seasonal variations of P_{max} and ϕ at canopy scale have also been readily observed in other temperate mixed forest sites, whereas they are not clearly observed in subtropical evergreen coniferous forests or evergreen broadleaf forests (Hollinger et al., 1999; Zhang et al., 2006). These studies suggested that the changes in temperature or LAI mainly controlled the seasonal changes of canopy P_{max} and ϕ. However, at our site we found that the correlations between LAI or temperature

and P_{max} and ϕ were not higher than those between VIs and P_{max} or ϕ. The ratio of LAI to P_{max} was different depending on the growth stage of the vegetation. It was higher in autumn than in spring, because leaves that had changed color, with reduced photosynthetic capacity, were still present on the plants in autumn.

Smith et al. (2002) observed a linear relationship between forest productivity and N concentration of canopy leaves independent of vegetation type. Furthermore, canopy N concentration correlates with the absorption rate for chlorophyll in the red region (around 680 nm) and blue region (around 490 nm), and the reflectance rate in the near-infrared region. This indicates the utility of VIs based on these bands, such as EVI, for estimating canopy N content and forest productivity.

Inoue et al. (2008) investigated the relationship between seasonal changes in P_{max} , ϕ and various spectral indices at an irrigated rice field. They report that P_{max} is correlated with RVI and other indices related to the wavelengths in chlorophyll a and b absorption region, and for ϕ, related to the wavelengths in blue region (450 nm) and infrared region (1330 nm).

Therefore, our results, together with those of others, identified RVI and/or EVI as available indices to assess photosynthetic parameters more directly, significantly, and effectively than LAI or air temperature, because they reflect the changes in canopy N or chlorophyll content. Either RVI or EVI can be used for estimating the seasonal variation of P_{max}, and here we selected RVI. The same analysis was conducted for EVI (Appendix B). We obtained the following empirical equations for the relationships between P_{max} (μmol CO_2 m^{-2} s^{-1}) and RVI, and ϕ (mol CO_2 [mol photon]$^{-1}$) and RVI, from the training data (Fig. 4):

Fig. 4

$$P_{max} = 3.65 \times \mathrm{RVI} - 3.35 \quad (7)$$

$$\phi = 0.005 \times \mathrm{RVI} - 0.001 \quad (8)$$

4.4 Short-term variations of P_{max} and ϕ, and the effects of meteorological factors

P_{max} and ϕ had large short-term variations (ΔP_{max} and $\Delta\phi$) during photosynthetically active periods (herein, $P_{max} > 20$ μmol CO_2 m^{-2} s^{-1}, and $\phi > 0.03$ mol CO_2 [mol photon]$^{-1}$). We analyzed the effects of four meteorological parameters on ΔP_{max} and $\Delta\phi$ for 3-day periods: daily temperature anomaly (ΔT, °C), relative solar radiation (rSR, %), maximum vapor pressure deficit (VPD, kPa), and soil water content (SWC, %). We used ΔT instead of daily mean temperature to remove the seasonal trend. Here, we defined ΔT as the difference between daily mean temperature and its 14-day running mean. We substituted rSR for the ratio of direct to diffuse radiation (Table 3).

Table 3

Fig. 5

We found a significant negative correlation between ΔP_{max} and rSR ($r = -0.49$, $P < 0.0001$) and with VPD ($r = -0.77$, $P < 0.0001$; Fig. 5a), and no significant relationship with either ΔT or SWC. When VPD was higher than about 1 kPa in summer, many examples of 'daytime depression' were observed at this site (Wang et al., 2004), because the higher VPD caused lower stomatal conductance and lower P_{max}. When both VPD and rSR were high on sunny days, photosynthesis became saturated in the upper layer of the canopy. Meanwhile, when VPD was low and rSR was low, ΔP_{max} was high. This suggested that on cloudy days diffuse radiation reached more deeply into the canopy and the photosynthetic capacity of the entire canopy was enhanced more than on sunny days. Our results agree with the diffuse enhancement reported by Gu et al. (2002). Both VPD and rSR had strong synergetic effects on ΔP_{max}. As VPD and rSR are correlated with each other, ΔP_{max} (μmol CO_2 m^{-2} s^{-1}) can be described by the effects of only VPD (kPa) (Fig. 5a) as:

$$\Delta P_{max} = -11.54 \times \mathrm{VPD} + 18.69 \qquad (9)$$

According to previous studies, for European beech forests, CO_2 uptake is high at VPD of 0.5-1 kPa, and CO_2 uptake is reduced when VPD becomes higher (Herbst et al., 2002). For Chinese evergreen coniferous forests, P_{max} reaches its maximum value when VPD is about 1.26 kPa and rapidly declines when VPD exceeds 2 kPa (Zhang et al., 2006). The optimum and threshold values of VPD probably differ for each vegetation type or canopy structure.

For $\Delta\phi$, significant correlation was found only with rSR ($r = -0.42$, $P < 0.0001$; Fig. 5b), and less significant correlations were shown with ΔT and VPD (Table3). After several consecutive sunny days, $\Delta\phi$ typically dropped suddenly. Exposure under strong direct solar radiation for few days possibly inhibited the canopy photosynthesis. In contrast, ϕ was enhanced when rSR was low, that is, when the proportion of diffuse radiation was high, similar to previous observations (Hollinger et al., 1994; Gu et al., 2002).

Thus, we verified that both direct irradiance and diffuse radiation affected $\Delta\phi$. We obtained the relationship between $\Delta\phi$ (mol CO_2 [mol photon]$^{-1}$) and rSR (%) (Fig. 5b) as:

$$\Delta\phi = -0.0002 \times \mathrm{rSR} + 0.0138 \qquad (10)$$

Although we expected that soil water content would have some effect on $\Delta\phi$, no significant correlation was observed. This may be because there was no severe drought stress during growing periods at this site during this study.

4.5 Estimation of P_{max}, ϕ and GPP

To determine P_{max} and ϕ using our new approach, we first estimated the seasonal variations (P_{max_season} and $\phi_{\_season}$) from their respective relationships with RVI (Eqs. (7) and (8)) on sunny days, using linear interpolation for other days.

Next, ΔP_{max} (μmol CO_2 m^{-2} s^{-1}) and $\Delta\phi$ (mol CO_2 [mol photon]$^{-1}$) were evaluated from VPD (kPa) and rSR (%) respectively (Eqs. (9) and (10)). Daily estimated P_{max} (est_P_{max} [μmol CO_2 m^{-2} s^{-1}]) was then determined as the sum of P_{max_season} and ΔP_{max}. The same process was used to determine est_ϕ.

Here, we define P_{max} and ϕ as previously approximated by fitting the light–response curve (Eq. (2)) as the "original" P_{max} and ϕ. P_{max_season} as determined from RVI was an underestimate compared to the original P_{max} (slope = 0.72 for P_{max_season} vs. original P_{max}). After applying the correction (ΔP_{max}), est_P_{max} was closer to the original (slope = 0.95 for est_P_{max} vs. original P_{max}; Table 4). Similarly,

Table 4

$\phi_{\_season}$ was underestimated by RVI compared with the original ϕ, and est_ ϕ was an improvement after applying the $\Delta\phi$ correction (slope of comparison increased from 0.66 before the correction to 0.78 after; Table 4). Thus, the effectiveness of the meteorological correction for both ΔP_{max} and $\Delta\phi$ was confirmed.

Finally, GPP was estimated by fitting est_P_{max} and est_ϕ to the light–response function at half-hour time steps. Diurnal changes of GPP were well expressed in relation to the light intensity (Fig. 6).

Fig. 6

GPP was precisely estimated from the parameters compared with observed GPP at half-hour time steps during the growing season in 2003-2004 (Table 5, Fig. 7). The slope of linear regression between observations and estimated GPP was 0.96 (R^2 = 0.83), and the standard error (SE) for the estimation was 4.21 μmol CO_2 m^{-2} s^{-1}. Also when the parameters were estimated using EVI, GPP was well estimated (slope = 0.95, R^2 = 0.84, SE = 4.23 μmol CO_2 m^{-2} s^{-1}), almost at the same precision as that by using RVI.

Table 5

Fig. 7

The GPP approximated by using the original parameters had a slope of 0.94 (R^2 = 0.87) when regressed against observed GPP; the SE was 3.67 μmol CO_2 m^{-2} s^{-1}. This is the implied regression error from using the light–response function. By our method, GPP tended to be about 4% of underestimate, and 83% of the half-hourly variations in observed GPP were explained by our model.

5. Conclusions

We propose a method for estimating GPP based on the light–response function that links remote sensing techniques and CO_2 flux measurement, from a plant physiological standpoint. With this method we parameterized P_{max} and ϕ as photosynthetic indicators consisting of both seasonal and short-term fluctuating components. The seasonal variations of P_{max} and ϕ had higher linear correlations with those of VIs such as RVI and EVI than with air temperature or LAI. Our results indicated that P_{max} and ϕ could be directly and adequately determined using either RVI or EVI. The

seasonality of P_{max} and ϕ seemed to correspond to the changing phenology of the vegetation, presumably reflecting canopy N or chlorophyll content.

In addition to seasonal patterns, we found that the short-term variations of P_{max} and ϕ were affected by VPD and the relative solar radiation, and we suggest the necessity of incorporating both seasonal and short-term variations into the estimation of P_{max} and ϕ. Assuming the use of satellite data, which are obtained under clear sky conditions, P_{max}, ϕ, and GPP would be underestimated without corrections for the effects of meteorological conditions.

Large numbers of parameters in models often cause uncertainty in estimated results, and ecosystem modeling has been in need of effective parameterization. We believe that the ability to generalize the relationships between P_{max}, ϕ, and RVI and/or EVI will contribute to ecosystem modeling. Both RVI and EVI showed strong correlations with P_{max}, and similarly with ϕ, and the GPP estimates from the parameters assessed by RVI or EVI were not very different. Further investigations involving different species and vegetation types should help to determine which VI is better to use for parameterization.

In this study, by using parameters of the light–response function that fluctuated daily, we demonstrated an improvement in providing accurate GPP estimates with high temporal resolution in response to diurnal, short-term, and seasonal changes. To further improve this method, we will also need additional studies of meteorological effects on the short-term variations in P_{max} and ϕ across various biomes and under severe conditions.

Acknowledgements

This study referred to some results from the Ministry of Environment Comprehensive Promotion Program for Global Environmental Research S1: “Research to develop a comprehensive carbon balance for Asian terrestrial ecosystems in preparation for 21st Century carbon management” (Principal Investigator: Takehisa Oikawa).

We express our appreciation to Dr. Hiroyuki Muraoka (Gifu University) and Dr. Ryuichi Hirata (Hokkaido University) for their valuable advice and to Dr. Koki Iwao (National Institute of Advanced Industrial Science and Technology) for technical support.

ZeGraph (http://www.zegraph.com/) was used for non-linear regression calculations, and we deeply appreciate the guidance and cooperation provided by Jiye Zeng.

Appendix A

We compared the RMSE from following three regression equations with the observed GPP:

1. *Michaelis-Menten's* rectangular hyperbolic equation:

$$\mathrm{GPP} = \frac{\phi \cdot \mathrm{PAR} \cdot P_{max}}{\left(\phi \cdot \mathrm{PAR} + P_{max}\right)} + Rd \qquad \text{(A.1)}$$

2. *Misterlich's* rectangular hyperbola:

$$\mathrm{GPP} = P_{max}\left(1 - e^{\left(\phi \cdot \mathrm{PAR}/P_{max}\right)}\right) + Rd \qquad \text{(A.2)}$$

Eq. A.1 and A.2 are used by Falge et al. (2001).

3. The non-rectangular hyperbola (Thornley, 1976; Eq. (2)) with θ fixed at 0.9.

The data set used and the method of calculation were the same as those mentioned in Section 3.3.

The averaged RMSE for each equation was, respectively, 3.16, 2.87, and 2.84 μmol CO_2 m^{-2} s^{-1}. Therefore, we chose the non-rectangular hyperbola, which had the smallest regression errors. With the *Michaelis-Menten* equation, values of regression coefficients often became unrealistic. The parameters of the *Misterlich* equation were highly correlated and comparable to those of the non-rectangular hyperbola. Regressions of parameters of the *Misterlich* equation and the non-rectangular hyperbola yielded slopes and intercepts of 1.06 and –0.36 (R^2 = 0.99), respectively, for P_{max} and 1.32 and 0.0 (R^2 = 0.95), respectively, for ϕ.

Appendix B

We obtained the following empirical equations for the relationships between P_{max} (μmol CO_2 m^{-2} s^{-1}) and EVI, from the training data:

$$P_{max} = 70.50 \times \text{EVI} - 9.03 \quad \text{(B.1)}$$

We found a significant negative correlation between ΔP_{max} (estimated by using EVI) and rSR (r = –0.52, $P < 0.0001$) and with VPD (r = –0.73, $P < 0.0001$), and no significant relationship with either ΔT (r = –0.18) or SWC (r = –0.03). ΔP_{max} (μmol CO_2 m^{-2} s^{-1}) can be described by the effects of only VPD (kPa) as:

$$\Delta P_{max} = -11.00 \times \text{VPD} + 19.28 \quad \text{(B.2)}$$

References

Baldocchi, D.D., Wilson, K.B., 2001. Modeling CO_2 and water vapor exchange of a temperate broadleaved forest across hourly to decadal time scales. Ecol. Model. 142 (1–2), 155–184.

Falge, E., Baldocchi, D.D., Olson, R, Anthoni, P., Aubinet, M., Bernhofer, C., Burba, G., Ceulemans, R., Clement, R., Dolman, H., Granier, A., Gross, P., Grunwald, T., Hollinger, D., Jensen, N.O., Katul, G., Keronen, P., Kowalski, A., Lai, C.T., Law, B.E., Meyers, T., Moncrieff, H., Moors, E., Munger, J.W., Pilegaard, K., Rannik, U., Rebmann, C., Suyker, A., Tenhunen, J., Tu, K., Verma, S., Vesala, T., Wilson, K., Wofsy, S., 2001. Gap filling strategies for defensible annual sums of net ecosystem exchange. Agric. Forest Meteorol. 107, 43–69.

Falge, E., Baldocchi, D.D., Tenhunen, J., Aubinet, M., Bakwin, P., Berbigier, P., Bernhofer, C., Burba, G., Clement, R., Davis, K.J., Elbers, J.A., Goldstein, A.H., Grelle, A., Granier, A., Guðmundsson, J., Hollinger, D., Kowalski, A.S., Katul, G., Law, B.E., Malhi, Y., Meyers, T., Monson, R.K., Munger, J.W., Oechel, W., Paw U, K.T, Pilegaard, K., Rannik, Ü., Rebmann, C., Suyker, A., Valentini, R., Wilson, K., Wofsy, S., 2002. Seasonality of ecosystem respiration and gross primary production as derived from FLUXNET measurements. Agric. Forest Meteorol. 113, 53–74.

Fujinuma, Y., Takada, M., Tashiro, K., Inoue, G., 2001. GHGs flux monitoring at Larch forest in Hokkaido, Japan. Proceedings of International Workshop for Advanced Flux Network and Flux Evaluation. Sapporo, Japan. pp.161–164

Gamon, J.A., Peñuelas, J., & Field, C.B., 1992. A narrow-waveband spectral index that tracks diurnal changes in photosynthetic efficiency. Remote Sens. Environ. 41, 35−44.

Gamon, J.A., Serrano, L., Surfus, J.S., 1997. The photochemical reflectance index: an optical indicator of photosynthetic radiation use efficiency across species, functional types and nutrient levels. Oecologia 112, 492–501.

Goward, S.N., Huemmrich, K.F., 1992. Vegetation canopy PAR absorptance and the normalized difference vegetation index–an assessment using the SAIL model. Remote Sens. Environ. 39 (2), 119–140.

Gu, L., Baldocchi, D., Verma, S.B., Black, T.A., Vesala, T., Falge, E.M., Dowty, P.R., 2002. Advantage of diffuse radiation for terrestrial ecosystem productivity. J. Geophys. Res. 107 (D6), 4050.

Herbst, M., Kutsch, W.L., Hummelshøj, P., Jensen, N.O., Kappen, L., 2002. Canopy physiology: interpreting the variations in eddy fluxes of water vapour and carbon dioxide observed over a beech forest. Basic Appl. Ecol. 3 (2), 157–169.

Hirano, T., Hirata, R., Fujinuma,Y., Saigusa, N., Yamamoto, S., Harazono, Y., Takada, M., Inukai, K., Inoue, G., 2003. CO_2 and water vapor exchange of a larch forest in northern Japan. Tellus 55B, 244–257.

Hirata, R., Hirano, T., Saigusa, N., Fujinuma, Y., Inukai, K., Kitamori, Y., Yamamoto, S., 2007. Seasonal and interannual variations in carbon dioxide exchange of a temperate larch forest. Agric. Forest Meteorol. 147, 110–124.

Hollinger, D.Y., Kelliher, F.M., Byers, J.N., Hunt, J.E., McSeveny, T.M. and Weir, P.L., 1994. Carbon dioxide exchange between an undisturbed old-growth temperate forest and the atmosphere. Ecology 75, 134–150.

Hollinger, D.Y., Goltz, S.M., Davidson, E.A., Lee, J.T., Tu, K., Valentine, H.T., 1999. Seasonal patterns and environmental control of carbon dioxide and water vapour exchange in an ecotonal boreal forest. Global Change Biol. 5, 891–902.

Huete, A., Didan, K., Miura, T., Rodriguez, E.P., Gao, X., Ferreira, L.G., 2002. Overview of the radiometric and biophysical performance of the MODIS vegetation indices. Remote Sens. Environ. 83, 195–213.

Inoue, Y., Peñuelas, J., Miyata, A., Mano, M., 2008. Normalized difference spectral indices for estimating photosynthetic efficiency and capacity at a canopy scale derived from hyperspectral and CO2 flux measurements in rice. Remote Sens. Environ. 112 (1), 156–172.

Jenkins, J.P., Richardson, A.D., Braswell, B.H., Ollinger, S.V., Hollinger, D.Y., Smith, M.-L., 2007. Refining light-use efficiency calculations for a deciduous forest canopy using simultaneous tower-based carbon flux and radiometric measurements. Agric. Forest Meteorol. 143, 64–79.

Kondo, J., Miura, A., 1983. Empirical formula of the solar radiation at the ground level and a simple method to examine an inaccurate pyranometer. Tenki 30, 469−475 (in Japanese).

Kosugi, Y., Tanaka, H., Takanashi, S., Matsuo, N., Ohte, N., Shibata, S., Tani, M. 2005. Three years of carbon and energy fluxes from Japanese evergreen broad-leaved forest. Agric. Forest Meteorol. 132, 329–343.

Lloyd, J., Taylor, J.A., 1994. On the temperature dependence of soil respiration. Funct. Ecol. 8, 315–323.

Monteith, J.L., 1972. Solar radiation and productivity in tropical ecosystems. J. Appl. Ecol. 9, 747–766.

Monteith, J.L., 1977. Climate and the efficiency of crop production in Britain. Philos. Trans. R. Soc. Lond. B. 281, 277–294.

Muraoka, H., Koizumi, H., 2005. Photosynthetic and structural characteristics of canopy and shrub trees in a cool-temperate deciduous broadleaved forest: implication to the ecosystem carbon gain. Agric. Forest Meteorol. 134, 39–59.

Myneni R.B., Nemani R.R., Running S.W., 1997. Estimation of global leaf area index and absorbed PAR using radiative transfer models. IEEE Trans. on Geosci. and Remote Sens. 35 (6), 1380–1393.

Nakaji, T., Oguma, H., Fujinuma, Y., 2006. Seasonal changes in the relationship between photochemical reflectance index and photosynthetic light use efficiency of Japanese larch needles. Int. Remote Sensing. 27, 493–509.

Nakaji, T., Ide, R., Oguma, H., Saigusa, N., Fujinuma, Y., 2007. Utility of spectral vegetation index for estimation of gross CO_2 flux under varied sky conditions. Remote Sens. Environ. 109 (3), 274–284.

Nakaji, T., Ide, R., Takagi, K.,Kosugi, Y., Ohkubo, S., Nasahara, K.N., Saigusa, N., Oguma, H., 2008. Utility of spectral vegetation indices for estimation of light conversion efficiency in coniferous forests in Japan. Agric. Forest Meteorol. 148, 776–787.

Nemoto, J., Shimada, M., Kobayashi, T., Arakawa, S., Yamashita, S., Watanabe, K., Sekiguchi, T., 1982. Illastrated meteorology. Asakura Publishing p.115(in Japanese).

Nichol, C.J., Rascher, U., Matsubara, S., Osmond, B., 2006. Assessing photosynthetic efficiency in an experimental mangrove canopy using remote sensing and chlorophyll fluorescence. Trees. 20, 9-15.

Potter, C.S., Randerson, J.T., Field, C.B., Matson, P.A., Vitousek, P.M., Mooney, H.A., Klooster, S.A., 1993. Terrestrial ecosystem production: a process model based on global satellite and surface data. Global Biogeochem. Cycles 7, 811–841.

Prince S.D., Goward S.N., 1995. Global primary production: a remote sensing approach. J. Biogeogr. 22 (4–5), 815–835.

Reich, P.B., Kloeppel, B.D., Ellsworth, D.S., Walters, M.B., 1995. Different photosynthesis–nitrogen relations in deciduous hardwood and evergreen coniferous tree species. Oecologia 104, 24–30.

Reich, P.B., Ellsworth, D.S., Walters, M.B., Vose, J. M., Gresham, C., Volin, J. C., Bowman, W. D., 1999. Generality of leaf trait relationships: a test across six biomes. Ecology 80, 1955–1969.

Rouse, J.W., Haas, R.H., Schell, J.A., Deering, D.W., Harlan, J.C., 1974. Monitoring the vernal advancement of retrogradation of natural vegetation. NASA/GSFC, Type 3, Final Report, Greenbelt, MD, pp. 371.

Ruimy, A., Jarvis, P.G., Baldocchi, D.D., Saugier, B., 1995. CO_2 fluxes over plant canopies and solar radiation: a review. Adv. Ecol. Res. 26, 1–69.

Saigusa, N., Yamamoto, S., Hirata, R., Ohtani, Y., Ide, R., Asanuma, J., Gamo, M., Hirano, T., Kondo, H., Kosugi, Y., Li S.G., Nakai, Y., Takagi, K., Tani, M., Wang, H., 2008. Temporal and spatial variations in the seasonal patterns of CO_2 flux in boreal, temperate, and tropical forests in East Asia. Agric. Forest Meteorol. 148, 700–713.

Saito, M., Maksyutov, S., Hirata, R., Richardson, A.D., 2009. An empirical model simulating diurnal and seasonal CO_2 flux for diverse vegetation types and climate conditions. Biogeosciences. 6, 585–599.

Sellers, P.J., Berry, J.A., Collatz, G.J., Field, C.B., Hall, F.G., 1992. Canopy reflectance, photosynthesis, and transpiration: 3. A reanalysis using improved leaf models and a new canopy integration scheme. Remote Sens. Environ. 42 (3), 187–216.

Sims, D.A., Gamon, J.A., 2002. Relationships between leaf pigment content and spectral reflectance across a wide range of species, leaf structures and developmental stages. Remote Sens. Environ. 81, 337–354.

Sims, D.A., Rahman, A.F., Cordova, V.D., Baldocchi, D.D., Flanagan, L.B., Goldstein, A.H., Hollinger, D.Y., Misson L., Monson, R.K., Shmid, H.P., Wofsy, S.C., Xu, L., 2005. Midday values of gross CO_2 flux and light use efficiency during satellite overpasses can be used to directly estimate eight-day mean flux. Agric. Forest Meteorol. 131, 1–12.

Sims, D.A., Luo, H., Hastings, S., Oechel, W.C., Rahman, A.F., Gamon, J.A., 2006. Parallel adjustments in vegetation greenness and ecosystem CO_2 exchange in response to drought in a Southern California chaparral ecosystem. Remote Sens. Environ. 103, 289–303.

Smith, M.L., Ollinger, S.V., Martin, M.E., Aber J.D., Hallett R.A., Goodale C.L., 2002. Direct estimation of aboveground forest productivity through hyperspectral remote sensing of canopy nitrogen. Ecol. Appl. 12 (5), 1286–1302.

Thornley, J.H.M., 1976. Mathematical Models in Plant Physiology. Academic Press, London, p. 318.

Tucker, C.J., 1979. Red and photographic infrared linear combinations for monitoring vegetation. Remote Sens. Environ. 8, 127-150.

Wang, H., Saigusa, N., Yamamoto, S., Kondo, H., Hirano, T., Toriyama, A., Fujinuma, Y., 2004. Net ecosystem CO_2 exchange over a larch forest in Hokkaido, Japan. Atmos. Environ. 38, 7021–7032.

Wright, I.J., Reich P.B., Westoby, M., Ackerly, D.D., Baruch, Z., Bongers, F., Cavender-Bares, J., Chapin, T., Cornelissen, J.H.C., Diemer, M., Flexas, J., Garnier, E., Groom, P.K., Gulias, J., Hikosaka, K., Lamont, B.B., Lee, T., Lee, W., Lusk, C., Midgley, J.J., Navas, M.L., Niinemets, U., Oleksyn, J., Osada, N., Poorter, H., Poot, P., Prior, L., Pyankov V.I., Roumet C., Thomas S.C., Tjoelker M.G., Veneklaas E.J., Villar R., 2004. The worldwide leaf economics spectrum. Nature 428 (6985), 821–827.

Yoder, B.J., Pettigrew-Crosby, R.E., 1995. Predicting nitrogen and chlorophyll content and concentrations form reflectance spectra (400–2500 nm) at leaf and canopy scales. Remote Sens. Environ. 53, 199–211.

Zhang, L-M., Yu, G-R., Sun, X-M, Wen, X-F., Ren, C-Y., Fu, Q-K., Li, Z-Q., Liu, Y-F., Guan, D-X., Yan, J-H., 2006. Seasonal variations of ecosystem apparent quantum yield (α) and maximum photosynthesis rate (P_{max}) of different forest ecosystems in China. Agric. Forest Meteorol. 137 (3–4), 176–187.

List of tables

List of figures

Fig. 5. Relationship between (a) ΔP_{max} with VPD (maximum vapor pressure deficit for 3-day periods, kPa), n = 106, and (b) $\Delta\phi$ and rSR (relative solar radiation, %), n = 127. Solid lines are regression lines.

Fig. 6. Diurnal changes of estimated GPP and observed GPP at half-hourly time steps (from day of year 229-234 in 2004).

Fig. 7. Relationship between observed GPP and GPP estimated using parameters derived from RVI at half–hourly time steps (for test data; n = 4025). Solid line is linear regression line; dashed line indicates $y = x$.

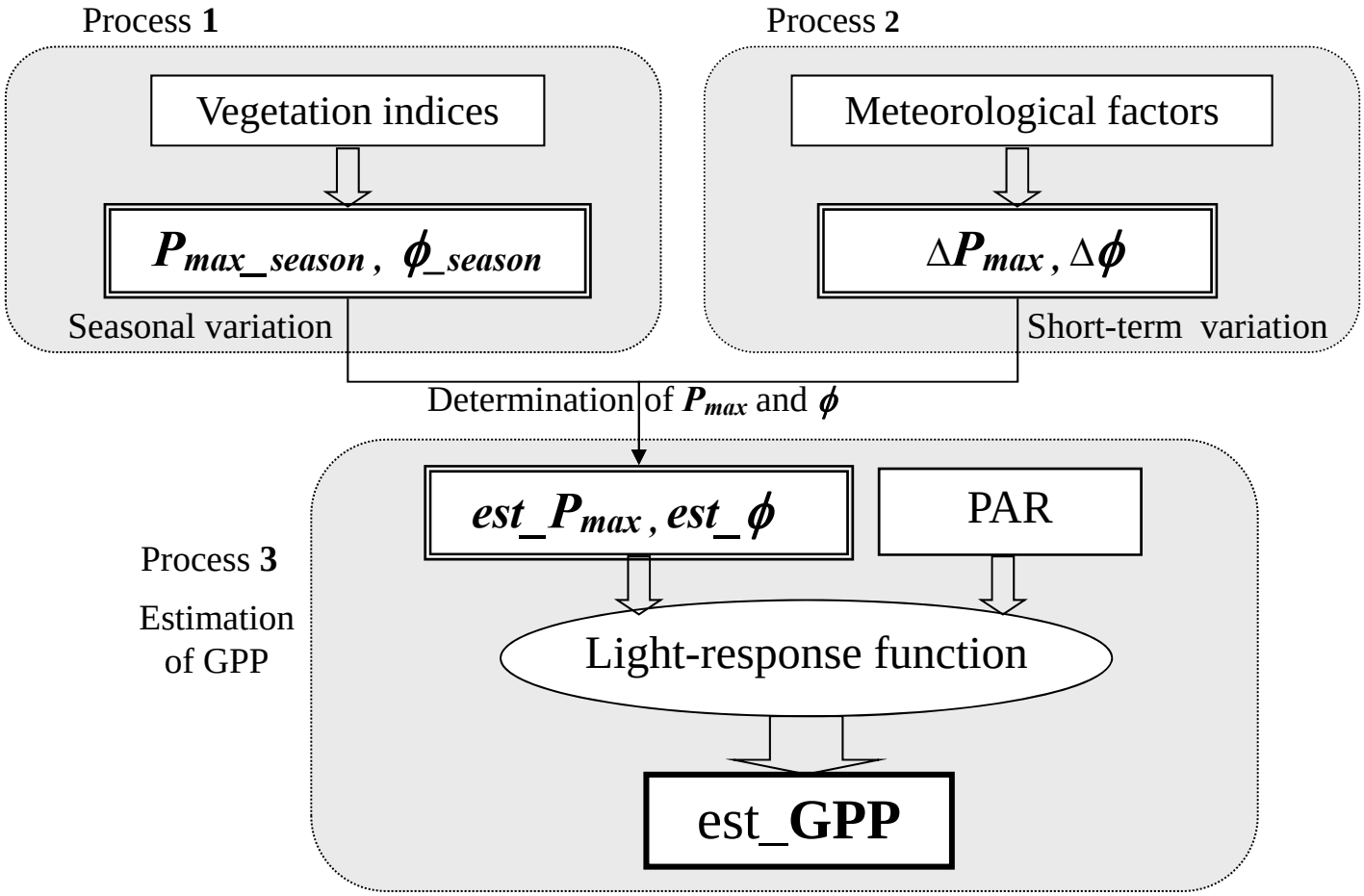

Fig. 1. Concept behind the determination of P_{max} and ϕ and the estimation of GPP. ▭ : input data, ▭ : parameters.

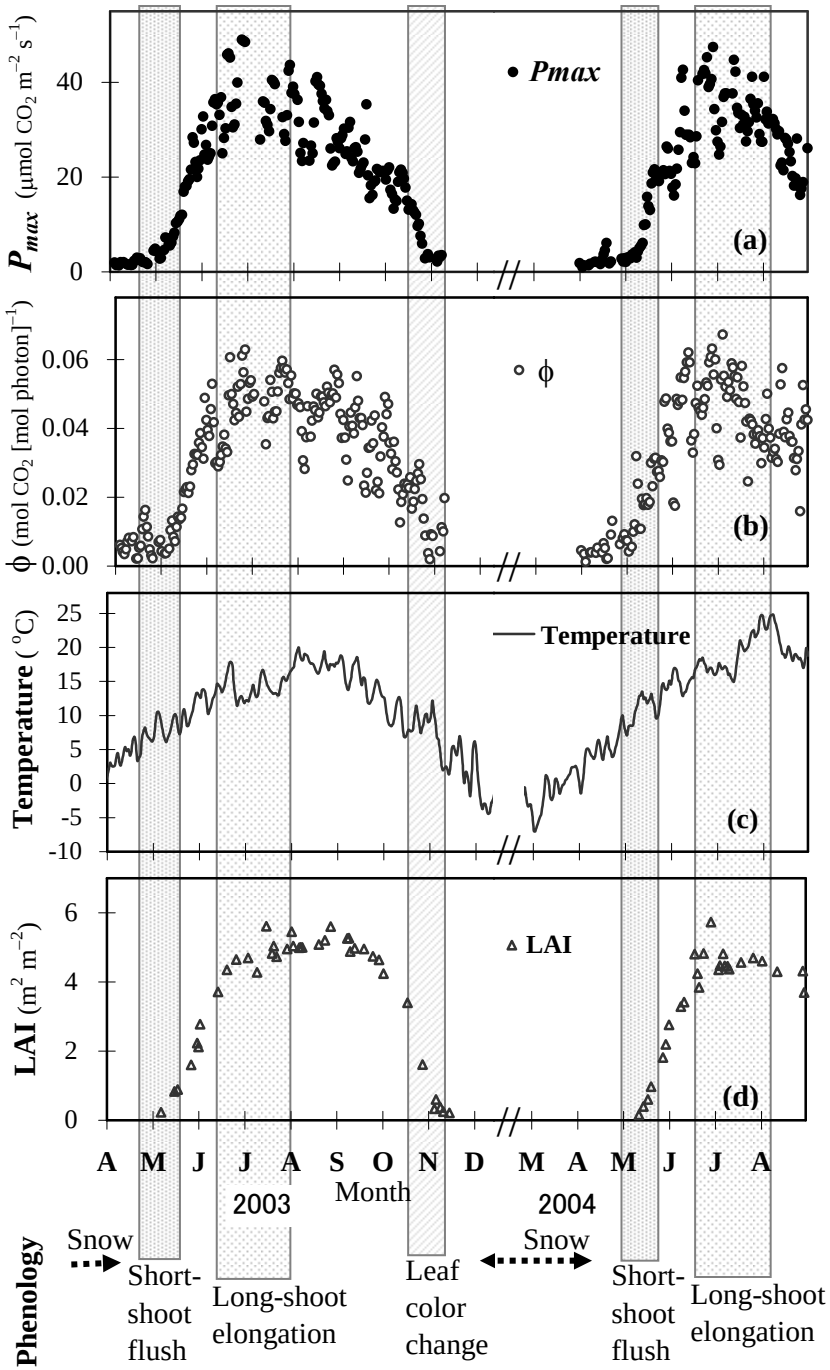

Fig. 2. Seasonal variations of (a) P_{max}, (b) ϕ, (c) temperature, (d) LAI and (superimposed) leaf phenology.

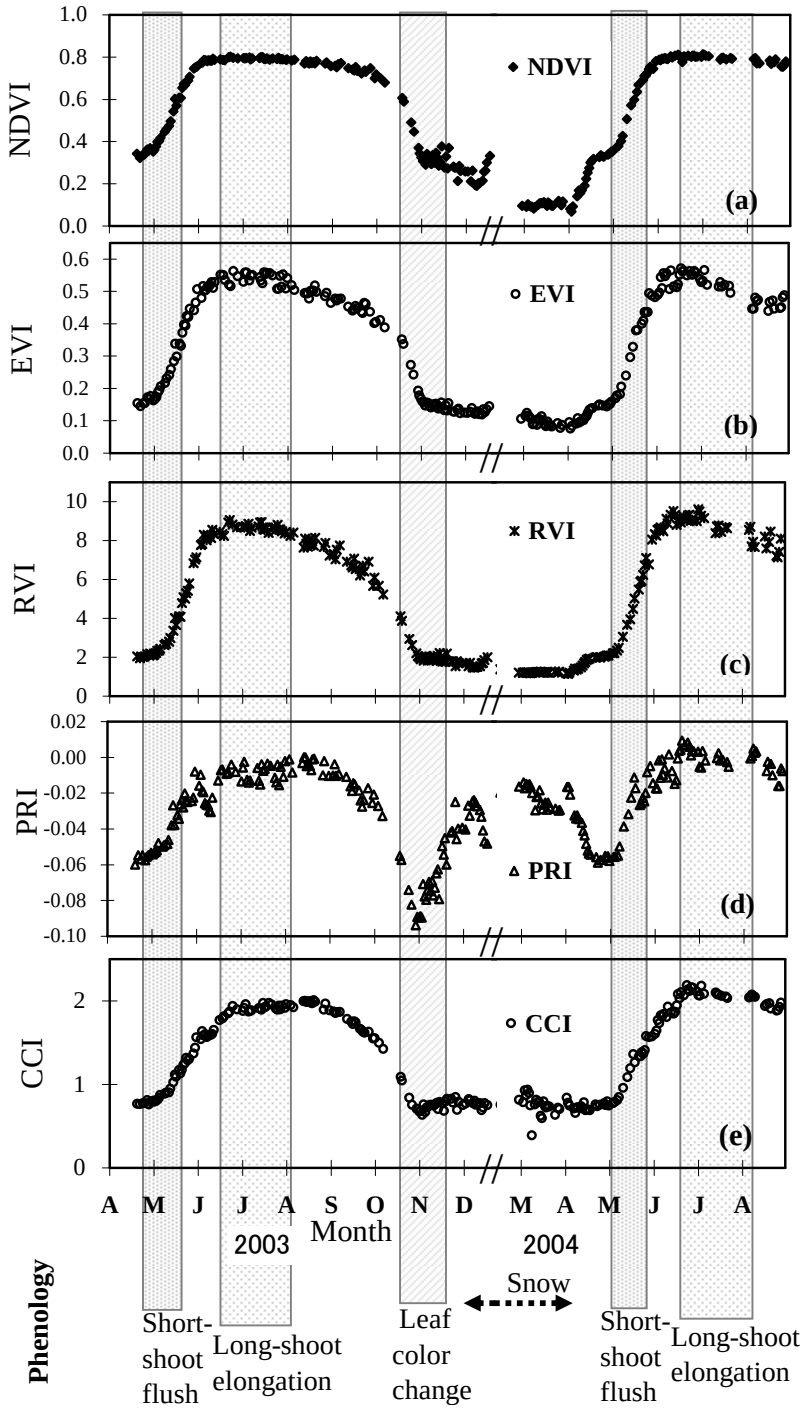

Fig. 3. Seasonal changes in vegetation indices: (a) NDVI, (b) EVI, (c) RVI, (d) PRI, and (e) CCI, with leaf phenology superimposed.

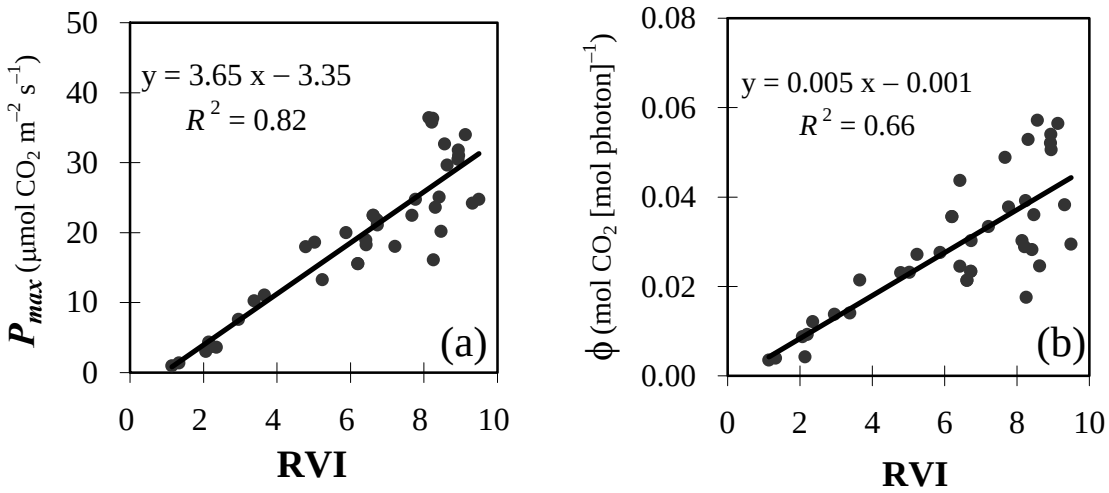

Fig. 4. Relationship between (a) P_{max} and RVI, and (b) ϕ and RVI using training data under clear sky conditions (n = 46).

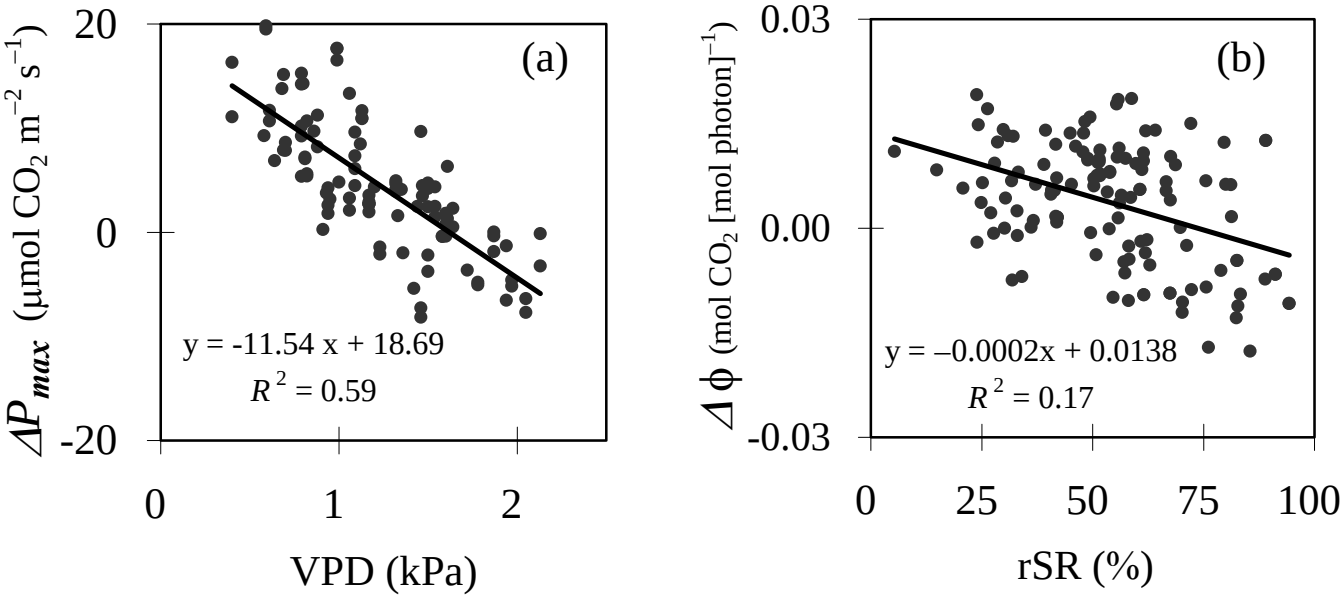

Fig. 5. Relationship between (a) ΔP_{max} with VPD (maximum vapor pressure deficit for 3-day periods, kPa), n = 106, and (b) $\Delta\phi$ and rSR (relative solar radiation, %), n = 127. Solid lines are regression lines.

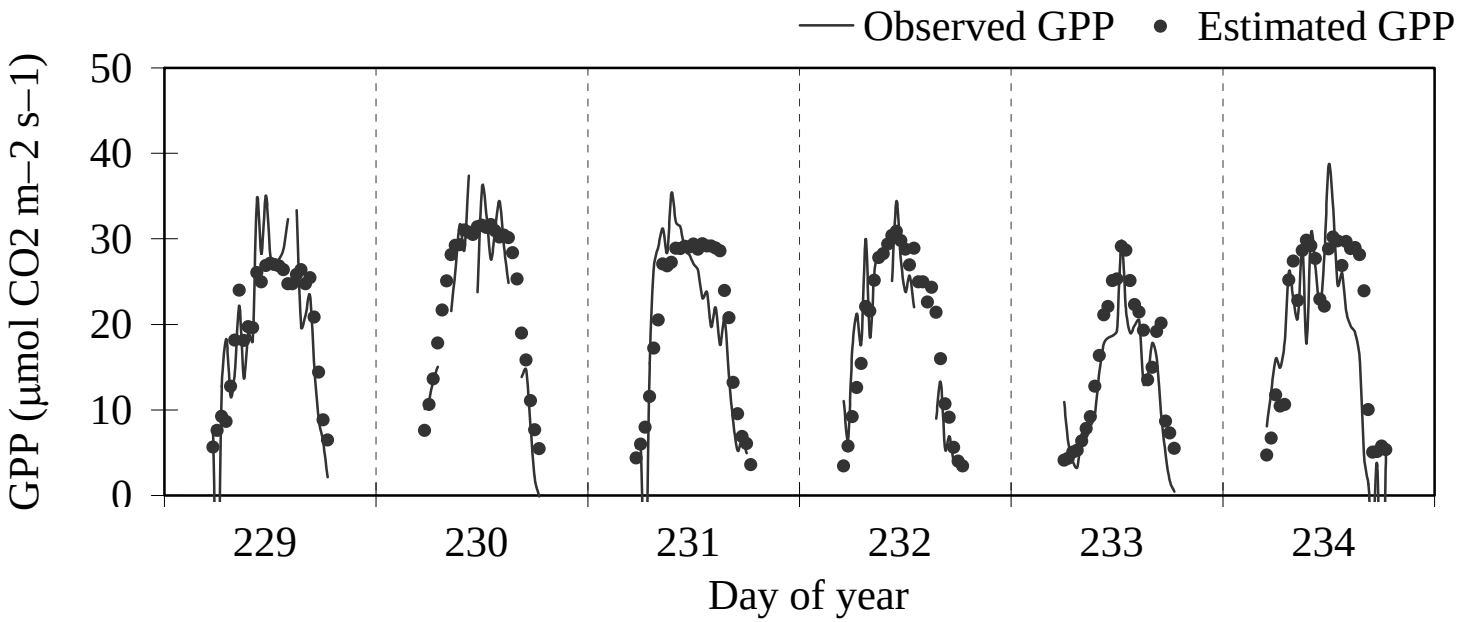

Fig. 6. Diurnal changes of estimated GPP and observed GPP at half-hourly time steps (from day of year 229-234 in 2004).

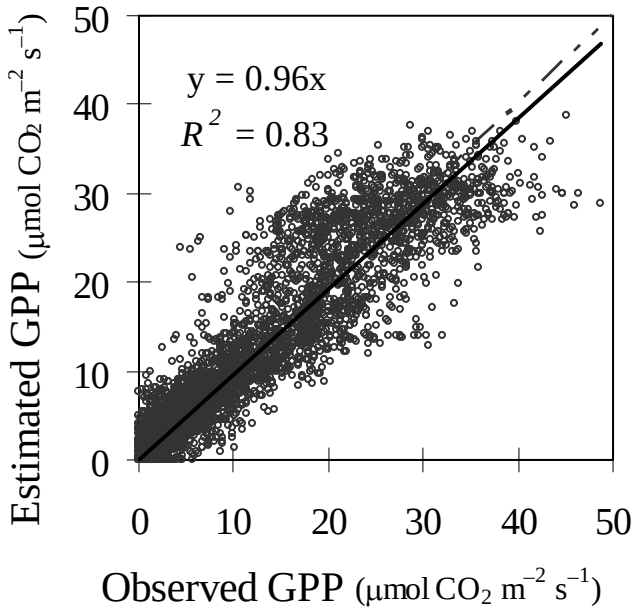

Fig. 7. Relationship between observed GPP and GPP estimated using parameters derived from RVI at half-hourly time steps (for test data; n = 4025). Solid line is regression line, and dashed line indicates y = x.

Table 1. Vegetation indices (VIs) used in this study.

VI	Formulation	Reference
NDVI (normalized difference vegetation index)	$(R_{nir} - R_{red})/(R_{nir} + R_{red})$	Tucker (1979)
EVI (enhanced vegetation index)	$2.5[(R_{nir} - R_{red})/(R_{nir} + 6.1R_{red} - 7.5R_{blue} + 1.0)]$	Huete et al. (2002)
RVI (ratio vegetation index, simple ratio)	R_{nir}/R_{red}	Rouse et al. (1974)
PRI (photochemical reflectance index)	$(R_{531} - R_{570})/(R_{531} + R_{570})$	Gamon et al. (1997)
CCI (canopy chlorophyll index)	D_{720}/D_{700}	Sims et al. (2006)

R_λ indicates spectral reflectance at wavelength around λ nm. $R_{nir} = R_{857}$, $R_{red} = R_{647}$, $R_{blue} = R_{464}$.
D_λ is the first derivative of reflectance at wavelengths around λ nm.

Table 2. Correlation coefficients (r) between P_{max}, ϕ and VIs, LAI and temperature under clear sky conditions (n = 88).

Parameter	P_{max}	ϕ
VI		
NDVI	0.88^{***}	0.78^{***}
EVI	0.92^{***}	0.79^{***}
RVI	0.92^{***}	0.81^{***}
PRI	0.74^{***}	0.63^{***}
CCI	0.88^{***}	0.77^{***}
LAI	0.67^{***}	0.60^{***}
Temperature	0.75^{***}	0.59^{***}

*** $p < 0.0001$ (Pearson's correlation test).

Table 3. Relationships between ΔP_{max}, $\Delta\phi$ and four meteorological factors: ΔT (temperature anomaly, ^{o}C), rSR (relative solar radiation, %), VPD (max vapor pressure deficit for 3-day periods, kPa), and SWC (soil water content, %).

Meteorological factor	ΔP_{max} (n = 105)	$\Delta\phi$ (n = 126)
ΔT	–0.16 *ns*	–0.24 *
rSR	–0.49 ***	–0.42 ***
VPD	–0.77 ***	–0.25 *
SWC	0.10 *ns*	–0.05 *ns*

*** p<0.0001, * p<0.01; *ns*: not significant (Pearson's correlation test).

Table 4. Relationships between estimated parameters and the original parameters (see text).

Estimated parameters	Slope	Intercept	R^2
P_{max_season}	0.72	3.56 (μmol CO_2 m^{-2} s^{-1})	0.83
est_P_{max}	0.95	1.54 (μmol CO_2 m^{-2} s^{-1})	0.88
$\phi_{\_season}$	0.66	0.009 (mol CO_2 [mol photon]$^{-1}$)	0.78
est_ϕ	0.78	0.007 (mol CO_2 [mol photon]$^{-1}$)	0.82

Seasonal parameters (P_{max_season}, $\phi_{\_season}$) were estimated by using RVI and corrected (est_P_{max}, est_ϕ) using meteorological factors (n = 171 for P_{max}, and n = 176 for ϕ).

Table 5. Regression parameters for comparison by linear regression of GPP estimated using three different parameter sets with observed GPP. GPP was estimated at half-hourly time steps (n = 4025).

Parameters used	Slope	R^2	SE (μmol CO_2 m^{-2} s^{-1})
Original parameters by light-response curve-fitting	0.94	0.87	3.67
Estimated P_{max} by RVI and ϕ by RVI	0.96	0.83	4.21
Estimated P_{max} by EVI and ϕ by RVI	0.95	0.84	4.23